ACS Photonics

pubs.acs.org/journal/apchd5

Letter

Distinguishing Small Molecules in Microcavity with Molecular Laser Polarization

Zhiyi Yuan, Xin Cheng, Yunke Zhou, Xiaotian Tan, Xuerui Gong, Hamim Rivy, Chaoyang Gong, Xudong Fan, Wen-Jie Wang, and Yu-Cheng Chen*

Cite This: *ACS Photonics* 2020, 7, 1908–1914

Read Online

ACCESS | Metrics & More | Article Recommendations | Supporting Information

ABSTRACT: Microlasers have emerged as a promising approach for the detection or identification of different biomolecules. Most lasers were designed to reflect changes of molecular concentration within the cavity, without being able to characterize biophysical changes in the gain medium. Here, we report a strategy to extract and amplify polarized laser emissions from small molecules and demonstrate how molecular rotation interplays with lasing at the nanoscale. The concept of molecular lasing polarization was proposed and was first evidenced to increase accordingly as the fluorophore binds to larger biomolecules in a microcavity. By detecting the molecular rotational correlation time through stimulated emission, small molecules could be distinguished, while conventional fluorescence polarization cannot. Theoretical models were developed to elucidate the underlying mechanisms. Finally, different types of small molecules were analyzed by adopting a Fabry-Pérot optofluidic laser. The results suggest an entirely new tool to quantify small molecules and guidance for laser emissions to characterize biophysical properties down to the molecular level.

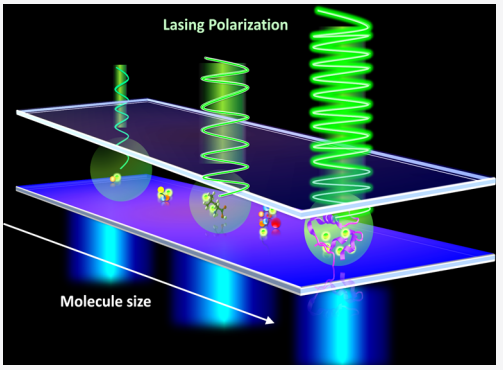

KEYWORDS: *microcavity, small molecules, lasing polarization, fluorescence polarization, lasers*

Optical resonators have become a powerful tool for biosensing since the past decade.[1−4] In particular, active resonators that utilize biological materials as the gain medium have shown tremendous potential to enhance specific features by labeling with fluorophores.[5−7] Thanks to the strong optical feedback provided by the cavity, even subtle changes in the gain induced by the underlying biological processes are significantly amplified, leading to a drastic change in the output emission characteristics. Recently, intracavity lasers have been demonstrated by using living cells,[7,11] DNA,[8,9] proteins,[10,11] virus,[12] and bacteria,[13] in which laser emissions are used to characterize biochemical changes within the cavity. The lasing intensity or wavelength changes accordingly as the binding concentrations increases.[14−17] In addition to concentrations, other physical features of molecules (molecular weight, polarization, structure, etc.) also play a critical role in molecular biology. As such, this study aims to explore how biophysical changes and physical properties within the gain medium may affect laser emissions.

Within the fields of molecular biology, small biomolecules are an indispensable part of the organism, which plays a crucial role in metabolic systems.[18] Quantitative detection and biological evaluation of small molecules have gained attention due to their promising applications in signaling and drug discovery.[19−21] When a small molecule binds to a fluorophore, the conjugated fluorophore exhibits a change in rotation speed that slightly alters the polarization degree of the fluorescence emission.[22,23] However, such subtle changes in polarization emission cannot be detected since the rotational correlation time of conjugated molecules is much smaller than the fluorescence lifetime.[24] In contrast, when conjugates are confined inside an optical cavity to form "stimulated emissions," the extremely short lifetime of stimulated emission (~100 ps[25]) becomes comparable to that of molecular rotational correlation time. Consequently, the effect of molecular rotation becomes significantly amplified, changing the degree of output laser polarization.[26]

In this work, we report a novel method to extract lasing polarization from small molecules by quantifying the effect of molecular rotational diffusion in a laser cavity. The proposed concept of slope efficiency ratio (SER $\eta_{\parallel}/\eta_{\perp}$) was employed as the sensing signal in which SER is defined as the ratio of lasing threshold slope between parallel polarized lasing (90°) and perpendicular polarized lasing (0°). (parallel: parallel to pump laser polarization; perpendicular: perpendicular to pump laser polarization.) For the first time, we investigated the underlying mechanism of molecular lasing polarization. Lasing polarization

Received: March 10, 2020
Published: July 23, 2020

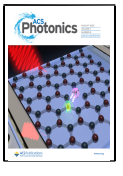

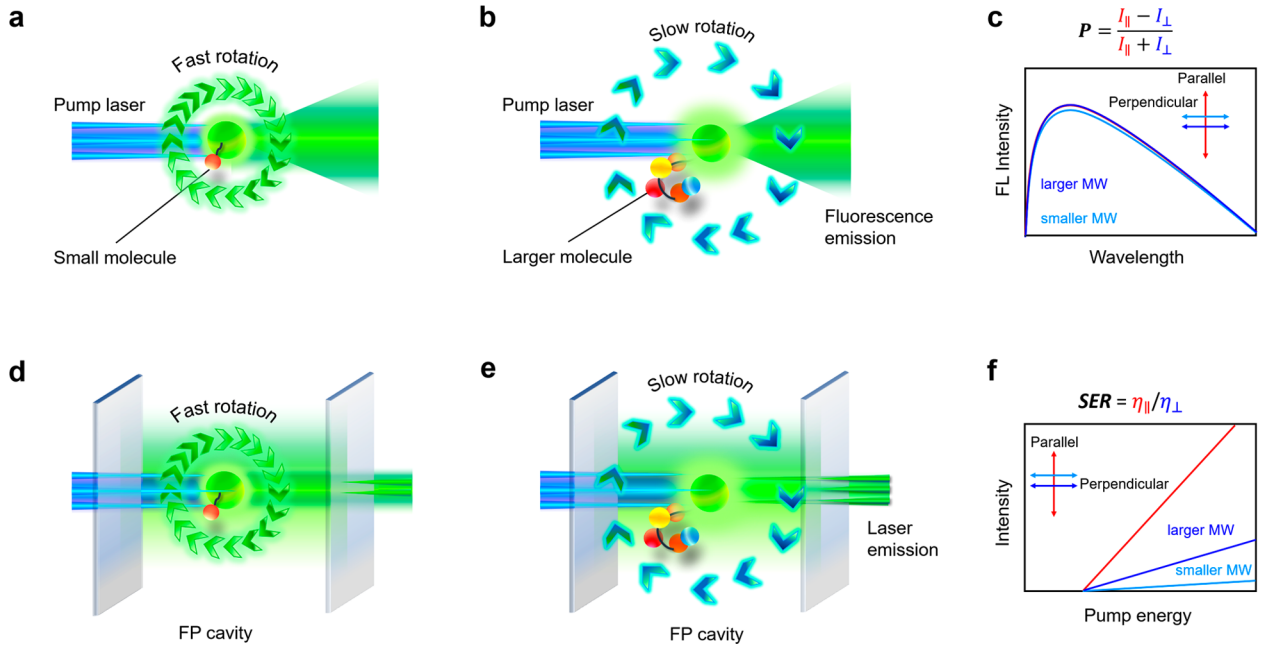

Figure 1. (a, b) Schematic diagram of conventional fluorescence polarization. Fluorescence emission is depolarized due to the rotational diffusion effect of dye molecules in the solution. When a small molecule binds to a fluorophore, the conjugated fluorophore slightly changes the polarization degree of the fluorescence emission. (c) Conceptual illustration of the fluorescence emission spectrum and conventional fluorescence polarization formula. Subtle changes in fluorescence emission cannot be detected. (d, e) Schematic diagram of molecular lasing polarization. In contrast to fluorescence polarization, the effect of small molecular rotation will be significantly amplified in the gain medium, changing the output laser polarization. (f) Conceptual illustration of slope efficiency ratio (SER $\eta_\parallel/\eta_\perp$), which is defined as the ratio of lasing threshold slope between parallel polarized lasing and perpendicular polarized lasing. Parallel: parallel to pump laser polarization; Perpendicular: perpendicular to pump laser polarization.

was found to increase accordingly, as the fluorophore binds to larger biomolecules. Theoretical models were carried out to elucidate our findings, which demonstrated the strong relationship between lasing polarizations and binding molecular weight. Finally, different types of small molecules were examined by adopting a Fabry-Pérot microcavity optofluidic laser. Our results reveal that small molecules could be clearly distinguished in lasing SER, while conventional fluorescence polarization cannot. Linearity between SER and molecular weight was attested to the potential for quantitative analysis.

Principle of Molecular Laser Polarization. Figure 1 shows the significance of lasing polarization by presenting the comparison between fluorescence and laser emissions upon binding to small molecules. Figure 1a–c clearly shows the limitation of conventional fluorescence polarization, where it cannot be used to identify small molecules (MW < 3000 Da). This is mainly due to the mechanism of fluorescence polarization, in which fluorescence emission remains depolarized when the fluorophore rotational correlation time is much shorter than the fluorescence lifetime. As such, tiny differences may not be detected for small molecule binding. In comparison, Figure 1d–f depicts the concept of a molecular lasing polarization. Different small molecules could be distinguished by their molecular weight, owing to the observable rotational correlation time change. The larger the molecule weight, the slower the rotation time, and hence, a stronger polarization will be amplified in the cavity.

In order to explain the mechanism of lasing polarization, we investigated the characteristics of rotational diffusion by employing a rate equation, as described in eqs 1–3.[27−29] The population dynamics of excited state molecules density is expressed as a function of angle θ and photon density in both parallel and perpendicular polarized orientation ($q_\parallel$ and $q_\perp$). Here, the θ represents the angle between the excitation pump polarization (Figure S1) and the fluorophore dipole orientation (Figure S2). Taking advantage of the coherence nature of stimulated emission, excited photons will only excite new photons with the identical polarization state. Consequently, the contrast between parallel and perpendicular polarized laser emissions are significantly enhanced.

$$\frac{dn(\theta)}{dt} = I_p\sigma_a \cos^2\theta\left(N_0 - \frac{\int_0^\pi n(\theta)\sin\theta d\theta}{2}\right) - \frac{n(\theta)}{\tau_f} - \frac{cq_\parallel}{m}\sigma_e n(\theta)\cos^2\theta + \frac{cq_\parallel}{m}\sigma_a\left(N_0 - \frac{\int_0^\pi n(\theta)\sin\theta d\theta}{2}\right)\cos^2\theta - \frac{cq_\perp}{m}\sigma_e n(\theta)\sin^2\theta + \frac{cq_\perp}{m}\sigma_a\left(N_0 - \frac{\int_0^\pi n(\theta)\sin\theta d\theta}{2}\right)\sin^2\theta + D\nabla^2 n \quad (1)$$

$$\frac{dq_\parallel}{dt} = -\frac{q_\parallel}{\tau_c} + \int_0^\pi \frac{c}{2mV}\sigma_e n(\theta)\cos^2\theta\sin\theta d\theta + \int_0^\pi \frac{cq_\parallel}{2m}\sigma_e n(\theta)\cos^2\theta\sin\theta d\theta - \int_0^\pi \frac{cq_\parallel}{2m}\sigma_a\left(N_0 - \frac{\int_0^\pi n(\theta)\sin\theta d\theta}{2}\right)\cos^2\theta\sin\theta d\theta \quad (2)$$

$$\frac{dq_\perp}{dt} = -\frac{q_\perp}{\tau_c} + \int_0^\pi \frac{c}{2mV}\sigma_e n(\theta)\sin^3\theta d\theta + \int_0^\pi \frac{cq_\perp}{2m}\sigma_e n(\theta)\sin^3\theta d\theta - \int_0^\pi \frac{cq_\perp}{2m}\sigma_a\left(N_0 - \frac{\int_0^\pi n(\theta)\sin\theta d\theta}{2}\right)\sin^3\theta d\theta \quad (3)$$

https://dx.doi.org/10.1021/acsphotonics.0c00387
ACS Photonics 2020, 7, 1908−1914

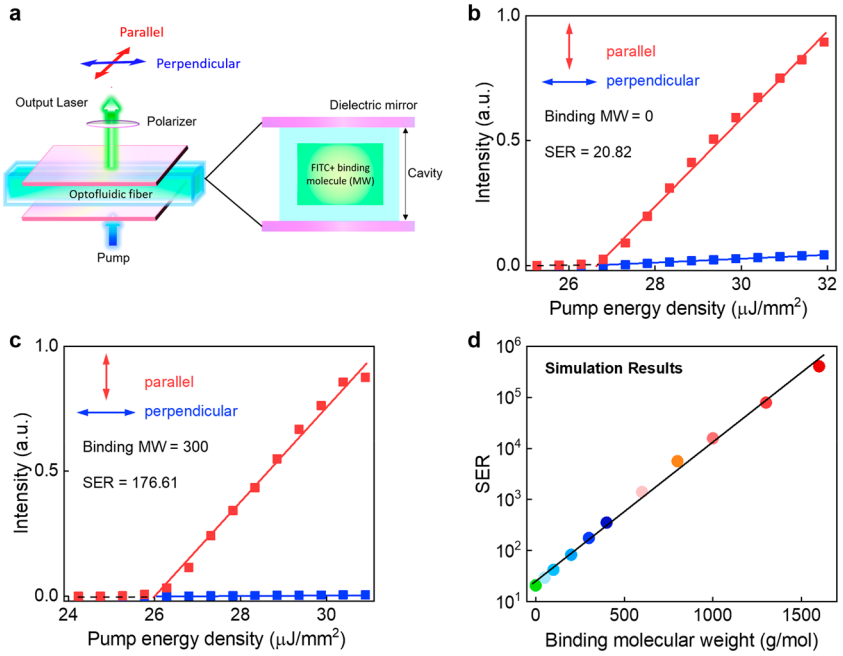

Figure 2. (a) Schematic diagram of the simulation and experimental setup. For all experiments, the dye concentration was fixed at 2 mM, the cavity length was fixed at 500 μm, and an excitation wavelength of 480 nm was used. Molecules with different molecular weights (MWs) binding to FITC were utilized as the laser gain. Both the parallel polarized laser and perpendicular polarized laser emissions were collected after passing through the polarizer. (b) Theoretically simulated laser output as a function of pump energy density for pure FITC, without binding molecule. (c) Theoretically simulated laser output as a function of pump energy density in the linear-log scale, binding with a small molecule (assumed to be 300 Da). Red dots represent the parallel polarized lasing output, blue dots represent the perpendicular polarized lasing output. (d) Theoretically simulated laser slope efficiency ratio (SER) as a function of binding molecular weight (MW) to FITC, the solid line is the log-linear fit.

Assuming that both parallel and perpendicular polarized orientation can achieve lasing under the condition of single mode at 550 nm, here we define $n(\theta)$, $q_{\parallel}$, and $q_{\perp}$ as the densities of dye molecules in the first excited state (for any θ), and the densities of the photons in parallel and perpendicular polarized orientation, respectively. σ_e and σ_a are the emission and absorption cross sections at the dye lasing wavelength. I_p is the time-dependent pump intensity, and N_0 is the concentration of dye molecules. c and m, respectively, describe the speed of light in vacuum and refractive index of the solvent. τ_c and τ_f, respectively, denote the photon lifetime in the cavity and fluorescence lifetime. The last term in eqns 2 and 3 represent the absorption of dye molecules. V is the mode volume and $D\nabla^2 n$ represents the rotational diffusion of excited state molecules according to the Fick's law (SI eq 16).[30] For detailed theory and calculation of lasing polarization, please refer to the Supporting Information. To simplify the calculations, we used eqs 4–6 to replace the above equations:

$$\frac{dn(\theta_i)}{dt} = I_p\sigma_{a0}\cos^2\theta_i\left(N_0 - \sum_{i=1}^{n} n(\theta_i)\right) - \frac{n(\theta_i)}{\tau_f} - \frac{cq_{\parallel}}{m}\sigma_e n(\theta_i)\cos^2\theta_i + \frac{cq_{\parallel}}{m}\sigma_a\left(N_0 - \sum_{i=1}^{n} n(\theta_i)\right)\cos^2\theta_i - \frac{cq_{\perp}}{m}\sigma_e n(\theta_i)\sin^2\theta_i + \frac{cq_{\perp}}{m}\sigma_a\left(N_0 - \sum_{i=1}^{n} n(\theta_i)\right)\sin^2\theta_i + \frac{D[n(\theta_{i+1}) - n(\theta_i)]}{(\pi/n)^2} - \frac{D[n(\theta_i) - n(\theta_{i-1})]}{(\pi/n)^2} + \frac{D}{\tan\theta(\pi/n)}[n(\theta_{i+1}) - n(\theta_i)] \quad (4)$$

$$\frac{dq_{\parallel}}{dt} = -\frac{q_{\parallel}}{\tau_c} + \frac{c}{mV}\sigma_e\sum_{i=1}^{n} n(\theta_i)\cos^2\theta_i + \frac{cq_{\parallel}}{m}\sigma_e\sum_{i=1}^{n} n(\theta_i)\cos^2\theta_i - \frac{cq_{\parallel}}{m}\sigma_a\left(N_0 - \sum_{i=1}^{n} n(\theta_i)\right)\sum_{i=1}^{n}\cos^2\theta_i \quad (5)$$

$$\frac{dq_{\perp}}{dt} = -\frac{q_{\perp}}{\tau_c} + \frac{c}{mV}\sigma_e\sum_{i=1}^{n} n(\theta_i)\sin^2\theta_i + \frac{cq_{\perp}}{m}\sigma_e\sum_{i=1}^{n} n(\theta_i)\sin^2\theta_i - \frac{cq_{\perp}}{2m}\sigma_e(N_0 - \sum_{i=1}^{n} n(\theta_i))\sum_{i=1}^{n}\sin^2\theta_i \quad (6)$$

Figure 2a illustrates the optical setup used in this work, where an optofluidic glass tube filled with Fluorescein (FITC) solution was sandwiched by two highly reflective dielectric mirrors to form Fabry-Pérot microcavity. A detailed description of mirror characterization, Fabry-Pérot cavity assembly, and the optical setup is given in the Methods section and Figure S3. All the molecule structures used were also provided in Figure S4. Herein the slope efficiency ratio (SER) was utilized as an analytical approach. Based on the derived theory and equations mentioned above, Figure 2b,c performs the simulation results of the laser output as a function of pump energy density with and without molecular binding. According to simulation, the calculated SER ($\eta_{\parallel}/\eta_{\perp}$) of FITC (without binding) is much lower than that of binding to a small molecule (MW ~ 300 Da) due to faster rotation speed. We further investigated the laser SER when binding to molecules with larger MWs in Figure 2d and surprisingly found a significant relationship between laser SER and binding MW.

Demonstration of Polarization between Small Molecules. The above simulation results reveal that the lasing SER increases exponentially with the MWs of the binding molecules. To validate our simulation results, we performed the experiment

https://dx.doi.org/10.1021/acsphotonics.0c00387
ACS Photonics 2020, 7, 1908–1914

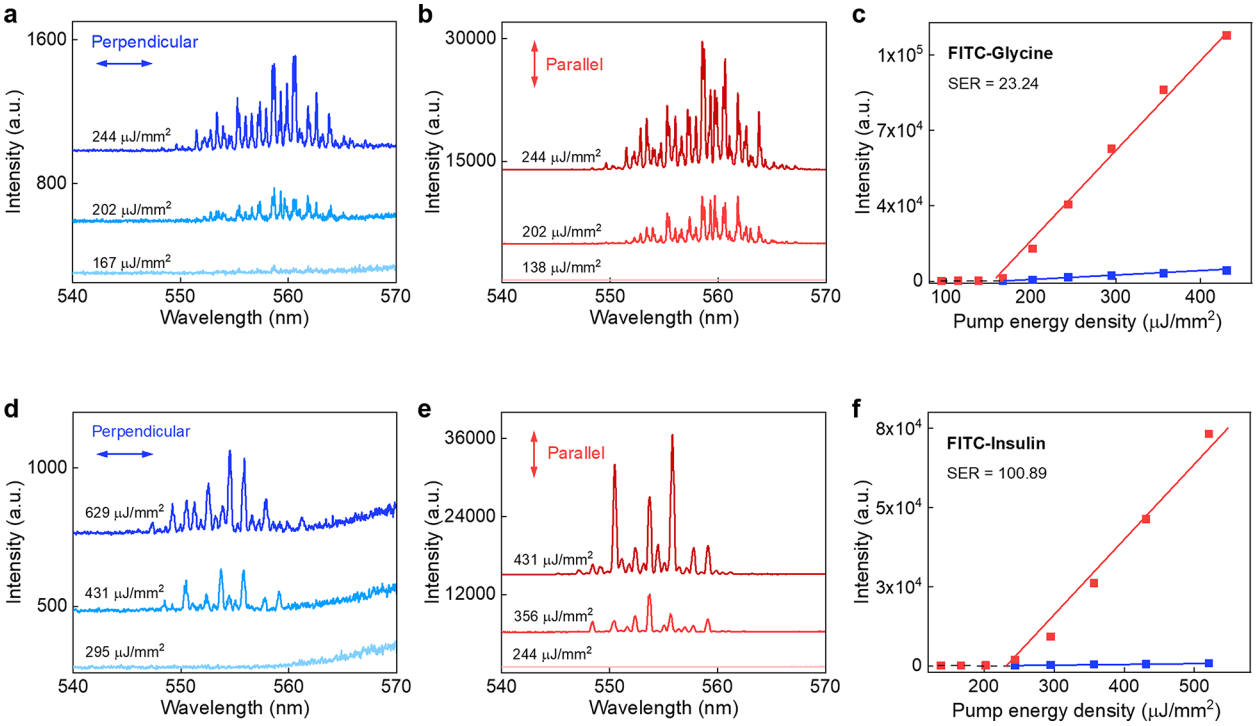

Figure 3. (a) Perpendicular polarized lasing spectra of 2-mM fluorescein (FITC) binding with glycine (MW = 75 g/mol); (b) Parallel polarized lasing spectra of 2-mM FITC binding with glycine. (c) Spectrally integrated FITC laser output as a function of pump energy density extracted from the spectra shown in (a) and (b), the solid lines denote a linear fit. (SER = 23.24). (d) Perpendicular polarized lasing spectra of 2 mM fluorescein (FITC) binding with insulin (MW = 3495 g/mol); (e) Parallel polarized lasing spectra of 2 mM FITC binding with insulin. (f) Spectrally integrated FITC laser output as a function of pump energy density extracted from the spectra shown in (d) and (e); the solid lines denote a linear fit. (SER = 100.89). Red dots represent the parallel polarized lasing output; blue dots represent the perpendicular polarized lasing output.

by using different sizes of molecules. In Figure 3a,b, we first demonstrate the polarized lasing spectra of FITC binding with glycine (MW = 75 Da) collected from the perpendicular and parallel directions, respectively. The threshold curves for both parallel and perpendicular are plotted in Figure S5a and b, respectively. The spectral line width was also evaluated below the threshold and above the threshold to confirm lasing behavior. Together, the spectrally integrated laser emission presented in Figure 3c shows the lasing SER is 23.24, resulting from the fast rotation of fluorophores. Next, in Figure 3d,e, we demonstrate the polarized lasing spectra of FITC binding with insulin (MW = 3495 Da) collected from the perpendicular and parallel directions, respectively. The threshold curves for both parallel and perpendicular are plotted in Figure S5c and d, respectively. The spectral line width was also evaluated below the threshold and above the threshold to confirm lasing behavior. By presenting together in Figure 3f, the perpendicularly polarized laser output energy is much lower than the parallel polarized orientation under the same pump energy density. Owing to the larger molecular weight (slower rotation) from insulin, a significantly larger lasing SER (100.89) was obtained. Therefore, the overall trend of SER is consistent with the theoretical simulation in Figure 2, signifying that lasing polarization can distinguish small molecules.

Distinguishing Amino Acids and Peptides. Going further, we investigated lasing SER as a function of binding MWs systematically. Herein, 10 different small molecules were selected, all of which have a molecular weight less than 3000 Da. Amino acids, small peptides, and polypeptides (Figures 4a and S4) with different MWs were conjugated with FITC to serve as laser gain medium. The threshold curves for both parallel and perpendicular emissions are plotted in Figures S6 and S7. As the spectral integrated intensity of perpendicular emission is much smaller than the parallel direction, individual threshold curves are provided in Figures S8 and S9 for better understanding. The spectral line width was also evaluated below the threshold and above the threshold to confirm lasing behaviors, respectively. The summary of laser SER resulting from ultrasmall molecules (MW < 500 Da) are displayed in Figure 4b, where small molecules with close molecular weights could still be distinguished. For small molecules with a larger size (500 Da < MW < 3000 Da), the lasing SER for respective molecules are presented in Figure 4c. The fitted lines in Figure 4b,c show the high linearity for all molecules, attesting to the potential application of laser polarization in small molecules. Most importantly, the lasing SER increased exponentially with the binding MW, which is consistent with the previous simulation results in Figure 2d.

To strengthen the significance of the proposed lasing polarization, we used the same method in Figure 4b,c to measure the ratio between the parallel and perpendicular fluorescence (fluorescence "SER"), as shown in Figure S10. As one can see, most of the molecules presented a SER close to 1, which is not distinguishable. In addition, we also measured the conventional fluorescence polarization resulting from different molecule-binding FITC in Figure 4d,e. By using the same molecules as for lasing polarization in Figure 4b,c, no significant trend was found in fluorescence polarization since the rotational correlation time is much lower than the fluorescence lifetime. To demonstrate that lasing SER can better reflect laser polarization characteristics than a traditional emission intensity ratio $((I_{\parallel} - I_{\perp})/(I_{\parallel} + I_{\perp}))$, we also plotted the relationship between the laser

https://dx.doi.org/10.1021/acsphotonics.0c00387
ACS Photonics 2020, 7, 1908−1914

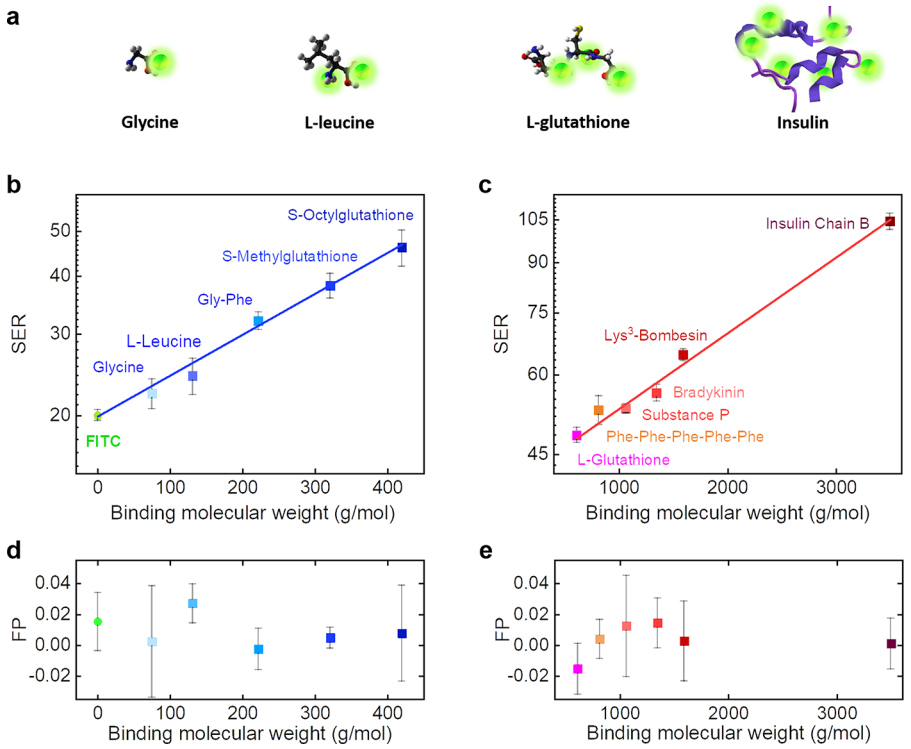

Figure 4. (a) 3D chemical structure of representative small molecules analyzed in this work (amino acids, peptides, tripeptides, and polypeptides). (b) Slope efficiency ratio (SER) as a function of binding molecular weight (MW < 500 Da) in the linear-log scale, including glycine (MW = 75 g/mol), L-leucine (MW = 131 g/mol), Gly-Phe (MW = 222 g/mol), *S*-methyglutathione (MW = 321 g/mol), *S*-octylglutathione (MW = 420 g/mol). (c) Slope efficiency ratio (SER) as a function of binding molecular weight (MW > 500 Da) in the linear-log scale, including L-glutathione (MW = 613 g/mol), Phe-Phe-Phe-Phe-Phe (MW = 814 g/mol), bradykinin (MW = 1060 g/mol), substance P (MW = 1348 g/mol), Lys^3-bombesin (MW = 1592 g/mol), insulin (MW = 3495 g/mol). The solid lines are linear fit. (d, e) Fluorescence polarization (FP) as a function of binding molecular weight corresponding to the same molecules mentioned in (b) and (c).

output polarization and the binding MW in Figure S11. Nonetheless, the laser output polarization shows significant errors and instabilities, making it extremely hard to discriminate different molecules. Finally, we sought to utilize this laser polarization system for small molecule sensing. As a proof-of-concept, small molecules with different concentrations were conducted for two representative-sized molecules in Figure S12a,b. Note that the rotational correlation time not only depends on the binding molecular weight, but also affects the ratio of bound molecules (bound molecules have larger rotational time than the unbound molecules). Consequently, when the concentration of target molecules increases, the rotational correlation time increases, resulting in larger SER values.

To avoid the effect of optical scattering, Figure S13 illustrates the same SER trend also observed with different water and glycerol ratios. Since glycerol provides higher viscosity than the water, which can slow down the rotation of fluorophores, this result verifies the increment of laser SER that is not due to the scattering of molecules, but the slower rotation of fluorophores.

CONCLUSION

In this study, we provided the first experimental evidence of molecular lasing polarization and demonstrated how lasing SER could be correlated to the study of small molecules. Taking advantage of strong optical feedback provided by the resonant cavity and coherence nature of stimulated emission, the effect of slight molecular rotation will be enlarged. Therefore, several types of small molecules could be clearly distinguished based on molecular mass as well as polarization degree. According to our theoretical model, molecular laser polarization may also be affected by the fluorophore, viscosity, or energy transfer. To the best of our knowledge, this is the first optical approach that can distinguish among different small molecules. This novel approach may have other applications in the biological and biochemical fields. We believe our investigation of molecular laser polarization may open a new avenue for laser emission-based detection to calibrate analytes.

METHODS

The experimental setup for all the experiments is shown in Figure 2. The transparent optofluidic glass tube (Friedrich and Dimmock Inc. (0.3 mm × 0.3 mm inner square cross-section, 0.1 mm wall thickness)), which contains FITC solution, was sandwiched by two highly reflective dielectric mirrors. The dye concentration is 2 mM, cavity length equals to 500 μm, with an excitation wavelength of 480 nm. For all measurements, we used the same mirrors, same pump location for different small molecular conjugated FITC solution, so that the Q-factor of the cavity kept at the equal value. Both the parallel polarized laser and perpendicularly polarized laser emissions were collected after passing through the polarizer. For the excitation of the Fabry-Pérot microcavity and the collection of laser emission, an inverted microscopic system (Nikon Ti_2) with 20× 0.4 NA objective was used. Optical pumping was achieved by a pulsed ns-laser (EKSPLA PS8001DR) integrated with an optical parametric oscillator (repetition rate: 50 Hz; pulse duration: 5 ns). According to the respective absorption wavelength of

https://dx.doi.org/10.1021/acsphotonics.0c00387
ACS Photonics 2020, 7, 1908−1914

fluorophores, the pump laser was tuned to 480 nm for FITC. The beam diameter at the objective focal plane was ∼16 μm wide. The collected light was sent into a charge-coupled device camera or an imaging spectrometer (Andor Kymera 328i and Newton 970 EMCCD).

Regarding materials, the dye Fluorescein (FITC) used in this work was purchased from Sigma-Aldrich (#3651). All the small molecules were purchased from Sigma-Aldrich, including glycine (#50046), L-leucine (#61819), Gly-Phe (#G2752), *S*-methylglutathione (#M4139), *S*-octylglutathione (#O5502), L-glutathione oxidized (#G4376), Phe-Phe-Phe-Phe-Phe acetate salt (#P3121), bradykinin acetate salt (#B3259), substance P (#S6883), [Lys^3]-bombesin (#B1647), and insulin (#I6383). To prepare the small molecular binding FITC solution, triethylammonium bicarbonate buffer (1.0 M, pH 8.5 ± 0.1) was selected as a buffer solution. First, 1.56 mg (4 μmol) of FITC was added to 1 mL of triethylammonium bicarbonate buffer. Second, amino acids or peptides were dissolved in triethylammonium bicarbonate buffer. Then, FITC solution was mixed with a small molecular solution with a ratio of 1:1. Finally, the mixed solution was incubated for 2 h before flowing into the optofluidic laser channel.

■ ASSOCIATED CONTENT

Supporting Information

The Supporting Information is available free of charge at https://pubs.acs.org/doi/10.1021/acsphotonics.0c00387.

Figures S1−S15 and Theory and Calculations (PDF)

■ AUTHOR INFORMATION

Corresponding Author

Yu-Cheng Chen − *School of Electrical and Electronic Engineering and School of Chemical and Biomedical Engineering, Nanyang Technological University, 639798, Singapore;* orcid.org/0000-0002-0008-5601; Email: yucchen@ntu.edu.sg

Authors

Zhiyi Yuan − *School of Electrical and Electronic Engineering, Nanyang Technological University, 639798, Singapore*

Xin Cheng − *School of Electrical and Electronic Engineering, Nanyang Technological University, 639798, Singapore*

Yunke Zhou − *School of Electrical and Electronic Engineering, Nanyang Technological University, 639798, Singapore*

Xiaotian Tan − *Department of Biomedical Engineering, University of Michigan, Ann Arbor, Ann Arbor, Michigan 48109, United States*

Xuerui Gong − *School of Electrical and Electronic Engineering, Nanyang Technological University, 639798, Singapore*

Hamim Rivy − *School of Electrical and Electronic Engineering, Nanyang Technological University, 639798, Singapore*

Chaoyang Gong − *School of Electrical and Electronic Engineering, Nanyang Technological University, 639798, Singapore*

Xudong Fan − *Department of Biomedical Engineering, University of Michigan, Ann Arbor, Ann Arbor, Michigan 48109, United States;* orcid.org/0000-0003-0149-1326

Wen-Jie Wang − *Key Lab of Advanced Transducers and Intelligent Control System of Ministry of Education, Taiyuan University of Technology, Taiyuan, Shanxi 030024, People's Republic of China*

Complete contact information is available at: https://pubs.acs.org/10.1021/acsphotonics.0c00387

Notes

The authors declare no competing financial interest.

■ ACKNOWLEDGMENTS

We would like to thank the lab support from Centre of Bio-Devices and Bioinformatics and Internal Grant NAP SUG-M4082308.040 from NTU.

■ REFERENCES

(1) He, L.; Ozdemir, K.; Zhu, J.; Kim, W.; Yang, L. Detecting single viruses and nanoparticles using whispering gallery microlasers. *Nat. Nanotechnol.* **2011**, *6*, 428−432.

(2) Baaske, M. D.; Foreman, M. R.; Vollmer, F. Single-molecule nucleic acid interactions monitored on a label-free microcavity biosensor platform. *Nat. Nanotechnol.* **2014**, *9* (11), 933.

(3) Arnold, S.; Khoshsima, M.; Teraoka, I.; Holler, S.; Vollmer, F. Shift of whispering-gallery modes in microspheres by protein adsorption. *Opt. Lett.* **2003**, *28* (4), 272−274.

(4) Vollmer, F.; Arnold, S.; Keng, D. Single virus detection from the reactive shift of a whispering-gallery mode. *Proc. Natl. Acad. Sci. U. S. A.* **2008**, *105*, 20701−20704.

(5) Fan, X.; Yun, S.-H. The potential of optofluidic biolasers. *Nat. Methods* **2014**, *11*, 141−147.

(6) Chen, Y. C.; Fan, X. Biological Lasers for Biomedical Applications. *Adv. Opt. Mater.* **2019**, *7* (11), 1900377.

(7) Humar, M.; Yun, S. H. Intracellular microlasers. *Nat. Photonics* **2015**, *9*, 572−576.

(8) Sun, Y.; Shopova, S. I.; Wu, C.-S.; Arnold, S.; Fan, X. Bioinspired optofluidic FRET lasers via DNA scaffolds. *Proc. Natl. Acad. Sci. U. S. A.* **2010**, *107*, 16039−16042.

(9) Chen, Q.; Chen, Y.-C.; Zhang, Z.; Wu, B.; Coleman, R.; Fan, X. An integrated microwell array platform for cell lasing analysis. *Lab Chip* **2017**, *17* (16), 2814−2820.

(10) Dietrich, C. P.; Steude, A.; Tropf, L.; Schubert, M.; Kronenberg, N. M.; Ostermann, K.; Höfling, S.; Gather, M. C. An exciton-polariton laser based on biologically produced fluorescent protein. *Sci. Adv.* **2016**, *2* (8), No. e1600666.

(11) Gather, M. C.; Yun, S. H. Single-cell biological lasers. *Nat. Photonics* **2011**, *5*, 406−410.

(12) Hales, J. E.; Matmon, G.; Dalby, P. A.; Ward, J. M.; Aeppli, G. Virus lasers for biological detection. *Nat. Commun.* **2019**, *10* (1), 11604-z.

(13) Jonáš, A.; Aas, M.; Karadag, Y.; Manioğlu, S.; Anand, S.; McGloin, D.; Bayraktar, H.; Kiraz, A. In vitro and in vivo biolasing of fluorescent proteins suspended in liquid microdroplet cavities. *Lab Chip* **2014**, *14*, 3093−3100.

(14) Gao, Z.; Zhang, W.; Yan, Y.; Yi, J.; Dong, H.; Wang, K.; Yao, J.; Zhao, Y. S. Proton-Controlled Organic Microlaser Switch. *ACS Nano* **2018**, *12*, 5734−5740.

(15) Yang, X.; Shu, W.; Wang, Y.; Gong, Y.; Gong, C.; Chen, Q.; Tan, X.; Peng, G.-D.; Fan, X.; Rao, Y.-J. Turbidimetric inhibition immunoassay revisited to enhance its sensitivity via an optofluidic laser. *Biosens. Bioelectron.* **2019**, *131*, 60−66.

(16) Chen, Y.-C.; Tan, X.; Sun, Q.; Chen, Q.; Wang, W.; Fan, X. Laser-emission imaging of nuclear biomarkers for high-contrast cancer screening and immunodiagnosis. *Nat. Biomed. Eng.* **2017**, *1* (9), 724−735.

(17) Yuan, Z.; Wang, Z.; Guan, P.; Wu, X.; Chen, Y. C. Lasing-Encoded Microsensor Driven by Interfacial Cavity Resonance Energy Transfer. *Adv. Opt. Mater.* **2020**, *8* (7), 1901596.

(18) Lane, A. N.; Fan, T. W.-M. Regulation of mammalian nucleotide metabolism and biosynthesis. *Nucleic Acids Res.* **2015**, *43*, 2466−2485.

(19) Zhang, J.; Allen, M. D. FRET-based biosensors for protein kinases: illuminating the kinome. *Mol. BioSyst.* **2007**, *3* (11), 759−65.

(20) Clark, B. A.; Alloosh, M.; Wenzel, J. W.; Sturek, M.; Kostrominova, T. Y. Effect of diet-induced obesity and metabolic syndrome on skeletal muscles of Ossabaw miniature swine. *Am. J. Physiol. Endocrinol. Metab.* **2011**, *300* (5), E848−E857.

(21) Ly, A.; Buck, A.; Balluff, B.; Sun, N.; Gorzolka, K.; Feuchtinger, A.; Janssen, K.-P.; Kuppen, P. J.; van de Velde, C. J.; Weirich, G.; et al. High-mass-resolution MALDI mass spectrometry imaging of metabolites from formalin-fixed paraffin-embedded tissue. *Nat. Protoc.* **2016**, *11* (8), 1428−1443.
(22) Zhang, Z.; Tang, C.; Zhao, L.; Xu, L.; Zhou, W.; Dong, Z.; Yang, Y.; Xie, Q.; Fang, X. Aptamer-based fluorescence polarization assay for separation-free exosome quantification. *Nanoscale* **2019**, *11* (20), 10106−10113.
(23) Glahn-Martínez, B.; Benito-Peña, E.; Salis, F.; Descalzo, A. B.; Orellana, G.; Moreno-Bondi, M. C. Sensitive rapid fluorescence polarization immunoassay for free mycophenolic acid determination in human serum and plasma. *Anal. Chem.* **2018**, *90* (8), 5459−5465.
(24) Lakowicz, J. R. *Principles of Fluorescence Spectroscopy*; Springer Science & Business Media, 2013.
(25) Bulovi, V.; Kozlov, V.; Khalfin, V.; Forrest, S. Transform-limited, narrow-linewidth lasing action in organic semiconductor microcavities. *Science* **1998**, *279* (5350), 553−555.
(26) Rivera, J. A.; Eden, J. G. Flavin mononucleotide biomolecular laser: longitudinal mode structure, polarization, and temporal characteristics as probes of local chemical environment. *Opt. Express* **2016**, *24* (10), 10858−10868.
(27) Yaroshenko, O. I. Theory of pulsed dye lasers with account of optical anisotropy and rotational diffusion. *J. Opt. A: Pure Appl. Opt.* **2003**, *5* (4), 328.
(28) Pikulik, L.; Yaroshenko, O. Polarization diagram for dye-based lasers. *J. Appl. Spectrosc.* **1977**, *27* (2), 986−990.
(29) Wang, X.; Linke, R.; Devlin, G.; Yokoyama, H. Lasing threshold behavior of microcavities: observation by polarization and spectroscopic measurements. *Phys. Rev. A: At., Mol., Opt. Phys.* **1993**, *47* (4), R2488.
(30) Weber, G., Rotational Brownian motion and polarization of the fluorescence of solutions. *Adv. Protein Chem.*; Elsevier, 1953; Vol. *8*, pp 415−459.

https://dx.doi.org/10.1021/acsphotonics.0c00387
ACS Photonics 2020, 7, 1908−1914